Measurement of Atmospheric Turbulence by Means of Light, Sound, and Radio Waves

Andreas Muschinski

Dept. of Electrical and Computer Engineering
University of Massachusetts Amherst

Observing the Turbulent Atmosphere:
Sampling Strategies, Technologies, and Applications
NCAR, Boulder, CO, 28-31 May 2008

Overview

- Introduction
- Wave propagation through turbulence: the basics
- Anisotropy in optical surface-layer turbulence
- Vertical-velocity biases observed with radars and sodars
- Outlook

Overview

- Introduction
- Wave propagation through turbulence: the basics
- Anisotropy in optical surface-layer turbulence
- Vertical-velocity biases observed with radars and sodars
- Outlook

Light, sound, and radio waves in the optically clear atmosphere

- Do not propagate along straight lines
- Change their amplitudes, phases, and angles-of-arrival deterministically and randomly in space and time
- Carry information about mean values and fluctuations of wind, temperature, density, pressure, humidity, and refractive index.

Differential downward ray-bending

can make the sun look squeezed …

… or otherwise deformed.

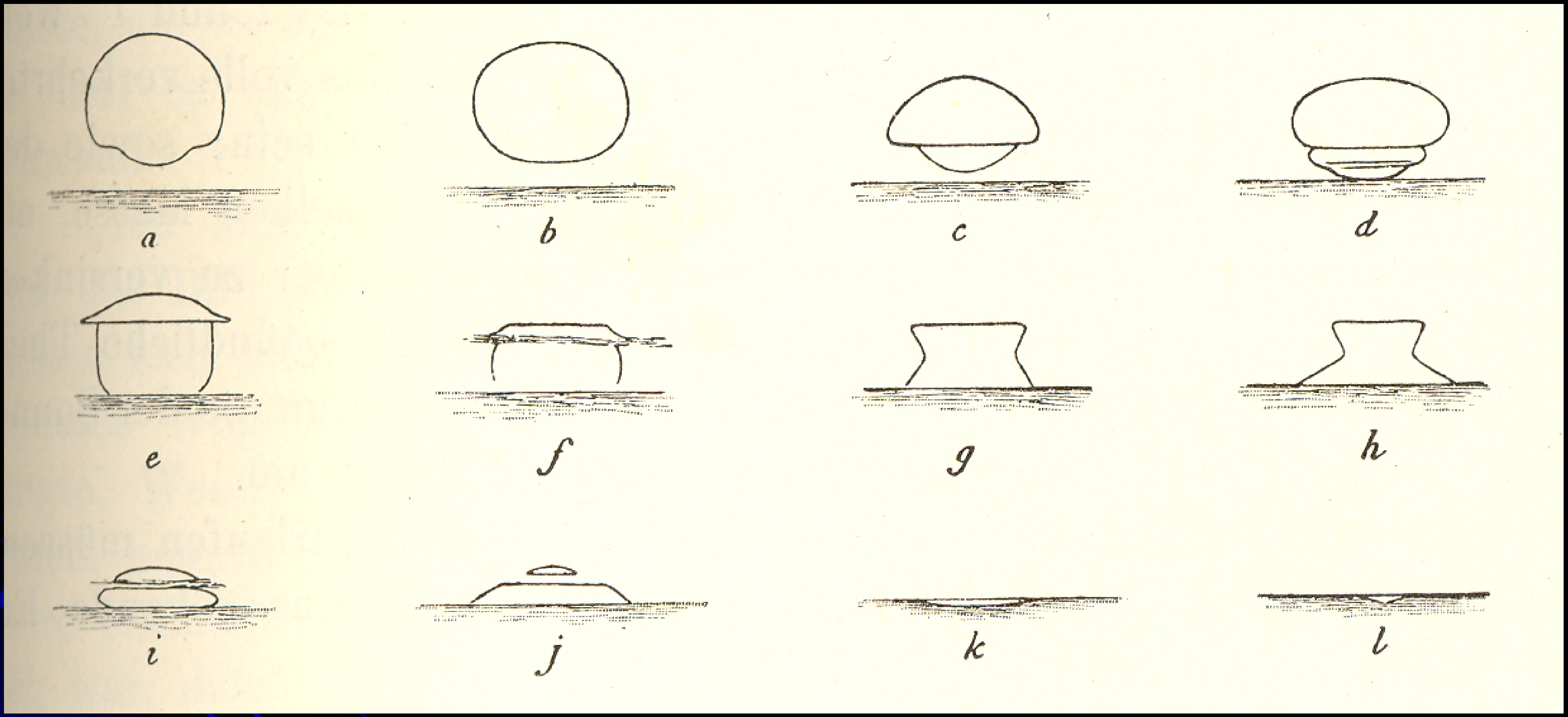

From Pernter and Exner, *Meteorologische Optik* (1910, p. 194)

Upward ray-bending can make

you see water puddles on a dry road …

Road mirage

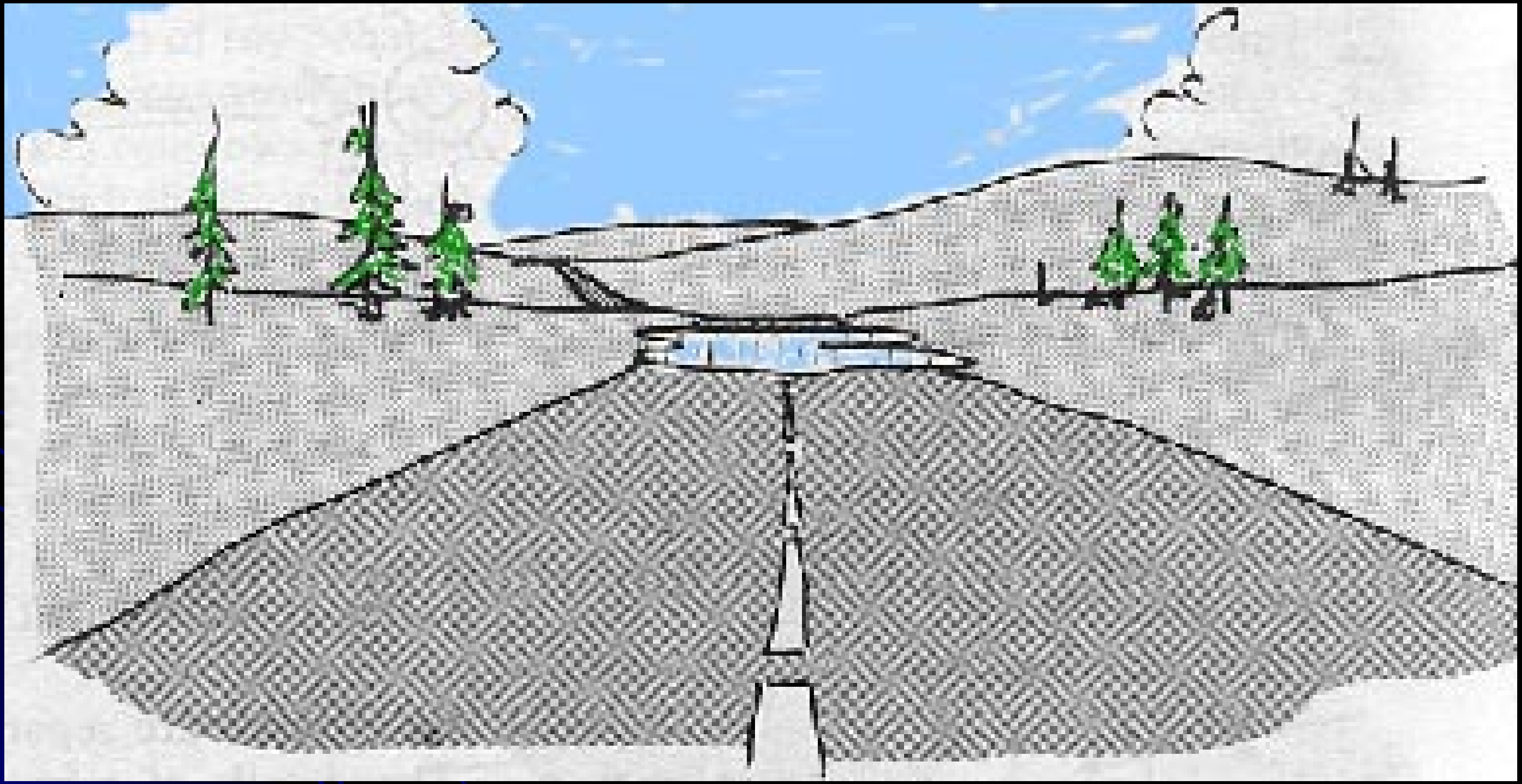

Near Bonneville Speedway, UT, August 2005

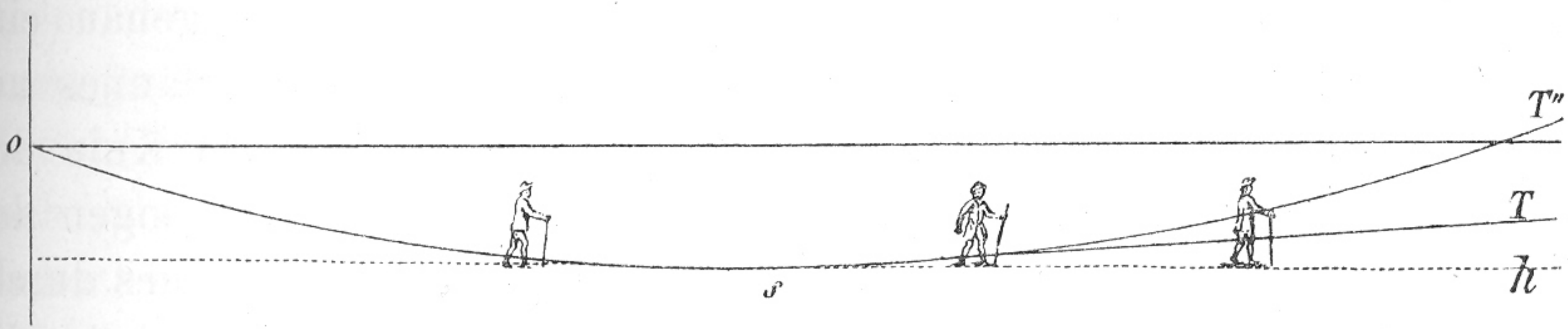

Fig. 33.

From Pernter and Exner, *Meteorologische Optik* (1910, p. 127)

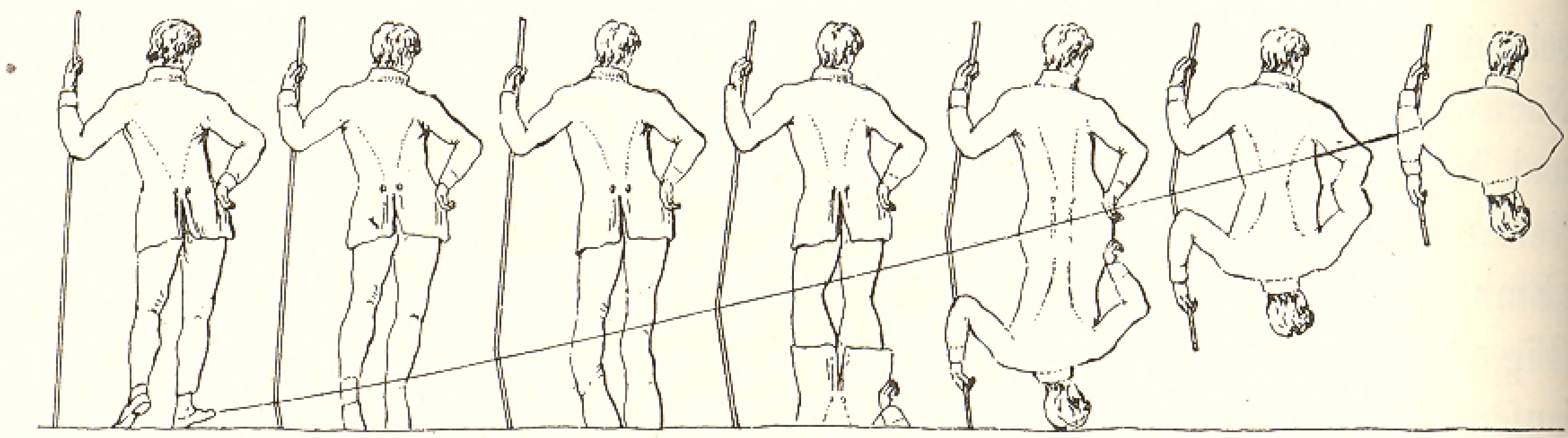

Fig. 34.

From Pernter and Exner, *Meteorologische Optik* (1910, p. 128)

Random ray-bending can create

changing patterns at the bottom of a swimming pool …

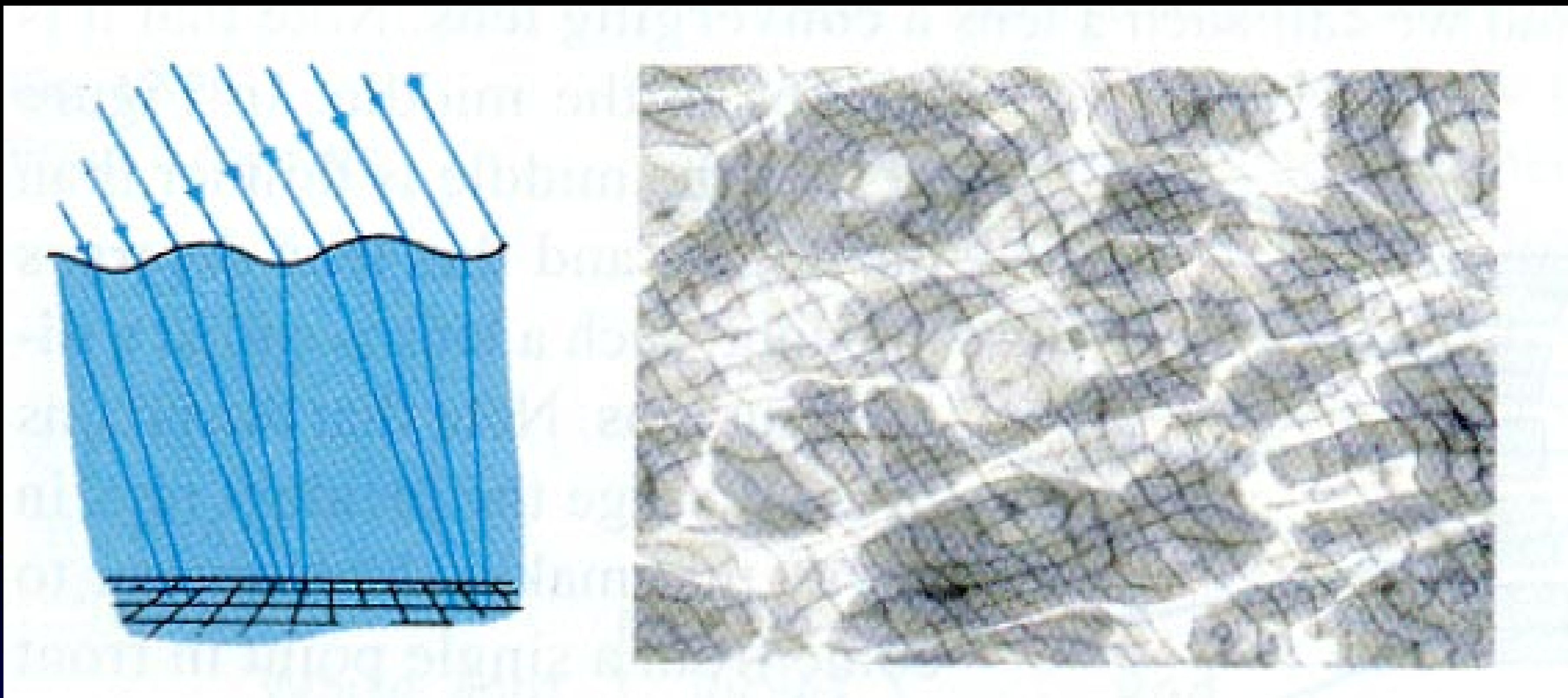

Overview

- Introduction
- Wave propagation through turbulence: the basics
- Anisotropy in optical surface-layer turbulence
- Vertical-velocity biases observed with radars and sodars
- Outlook

Valeryan Tatarskii

Tatarskii, V. I., 1961:
Wave Propagation in a Turbulent Medium.
McGraw-Hill, New York, 285 pp.

Tatarskii, V. I., 1971:
The Effects of the Turbulent Atmosphere on Wave Propagation.
Israel Program for Scientific Translation, Jerusalem, 472 pp.

Rytov, S. M., Y. A. Kravtsov, and V. I. Tatarskii, 1986-89:
Principles of Statistical Radiophysics, Vols. 1-4.
Springer, Berlin.

The inhomogeneous Helmholtz equation

- Maxwell equations
- Time-harmonic fields
- Simplified constitutive parameters ($\mu=\mu_0$, $\sigma=0$, ε varies with location)
- Wave equation
- (Inhomogeneous) Helmholtz equation

Methods to solve the inhomogeneous Helmholtz equation

- Eikonal equation
- Born approximation
- Rytov approximation
- Parabolic equation

Eikonal equation and transport equation

Consider scalar Helmholtz equation:

$$\nabla^2 E + k^2 \varepsilon_r E = 0, \tag{1}$$

where E is one of the three Cartesian components of the electrical field vector, k is the wave number of the unperturbed EM wave,

$$\varepsilon_r = n^2 \tag{2}$$

is the relative permittivity, and n is the refractive index.

Let $\varepsilon_r(\mathbf{r})$ be a deterministic or random field that is smoothly inhomogeneous, such that E is locally a plane wave,

$$\begin{aligned} E(\mathbf{r}) &= A(\mathbf{r}) \exp[iS(\mathbf{r})] \\ &= A(\mathbf{r}) \exp[ik\varphi(\mathbf{r})], \end{aligned} \tag{3}$$

where $A(\mathbf{r})$ is the amplitude, $S(\mathbf{r})$ is the phase,

$$\varphi(\mathbf{r}) = \frac{S(\mathbf{r})}{k} \tag{4}$$

is the eikonal (or "phase path").

Eikonal equation and transport equation (cont.'d)

Per definition of smooth inhomogeneity, the change of $A(\mathbf{r})$ and $\nabla S(\mathbf{r})$ over one EM wavelength is negligible ("locally plane waves").

Expand $E(\mathbf{r})$ in series of powers in $(ik)^{-1}$:

$$E(\mathbf{r}) = \left(A_0(\mathbf{r}) + \frac{A_1(\mathbf{r})}{ik} + \frac{A_2(\mathbf{r})}{(ik)^2} + \dots \right) \exp\left[ik\varphi(\mathbf{r})\right]. \tag{5}$$

Insert into Helmholtz equation, (1).

First term, proportional to $(ik)^2$, gives the **eikonal equation,**

$$\boxed{(\nabla\varphi)^2 = n^2.} \tag{6}$$

Second term, proportional to $(ik)^1$, gives the **transport equation,**

$$2\nabla A_0 \cdot \nabla\varphi + A_0 \nabla^2 \varphi = 0. \tag{7}$$

The eikonal equation and the transport equation are the equations for geometrical optics.

Refraction and diffraction

Eikonal equation (geometrical optics, “ray tracing”)	Born approximation
Describes refraction but not diffraction Approximates variances and frequency spectra of optical angle-of-arrival (AOA) fluctuations very well if aperture diameter is larger than twice the Fresnel length	Describes both refraction and diffraction Very good approximation for radio-wave backscatter from clear-air refractive-index perturbations Fraunhofer approximation valid if turbulence is Bragg-isotropic Fresnel approximation (or higher-order approximation) necessary if turbulence not Bragg-isotropic of in case of scatter from interfaces

Turbulence in the inertial range (in a nutshell)

Structure function of a random refractive-index field:

$$D_n(\mathbf{r}_1, \mathbf{r}_2) = \left\langle [n(\mathbf{r}_1) - n(\mathbf{r}_2)]^2 \right\rangle. \quad (1)$$

Locally homogeneous refractive-index field:

$$D_n = D_n(\mathbf{r}), \quad (2)$$

where $\mathbf{r} = \mathbf{r}_1 - \mathbf{r}_2$ is the spatial lag vector.

Locally homogeneous AND isotropic refractive-index field:

$$D_n = D_n(r), \quad (3)$$

where $r = |\mathbf{r}_1 - \mathbf{r}_2|$.

Inertial-range turbulence (Kolmorogov, Obukhov, 1941):

$$D_n(r) = C_n^2 r^{2/3}, \quad (4)$$

where C_n^2 is the **structure parameter**.

Three-dimensional wave-number spectrum for refractive-index fluctuations in the inertial range:

$$\Phi_n(\kappa) = \frac{5}{18\pi\Gamma(1/3)} C_n^2 \kappa^{-11/3} = 0.033\, C_n^2 \kappa^{-11/3}, \quad (5)$$

where $\kappa = \sqrt{\kappa_1^2 + \kappa_2^2 + \kappa_3^2}$.

Optical angle-of-arrival fluctuations
(from theory of eikonal fluctuations)

Consider vertical angle-of-arrival (AOA) fluctuations (local and instantaneous wave-front tilts) at point receiver located at distance L from source:

$$\alpha(y,z) = \frac{\partial}{\partial z}\left(\int_{x=0}^{L} n'(x,y,z)\,dx\right). \tag{1}$$

Variance of vertical AOA fluctuations of a **spherical wave** in locally homogeneous and isotropic turbulence, measured with two-point interferometer with baseline b:

$$\langle \alpha^2(b)\rangle = \frac{D_S(b)}{k^2 b^2}, \tag{2}$$

where

$$D_S(\rho) = 8\pi^2 L k^2 \int_0^\infty d\kappa \Phi_n(\kappa)\,\kappa \int_0^1 du\,[1 - J_0(\kappa\rho u)] \tag{3}$$

is the **phase structure function** of a spherical wave in the receiving plane. (Here, $u = x/L$.)

Variance of aperture-averaged AOA fluctuations (circular aperture with radius a)

$$\langle \overline{\alpha}^2\rangle = \frac{3}{8} 8\pi^2 L \int_0^\infty d\kappa \Phi_n(\kappa)\,\kappa^3 \left[\frac{J_1(\kappa a)}{\kappa a}\right]^2. \tag{4}$$

Evaluation gives

$$\langle \overline{\alpha}^2\rangle = 1.06\, C_n^2 L D^{-1/3}, \tag{5}$$

where $D = 2a$ is the aperture diameter.

Horse Farm, Amherst, MA, 19 June, 2005


MEADE
TOSHIBA
2005 6 19

“Seeing” the ground cooling after sunset

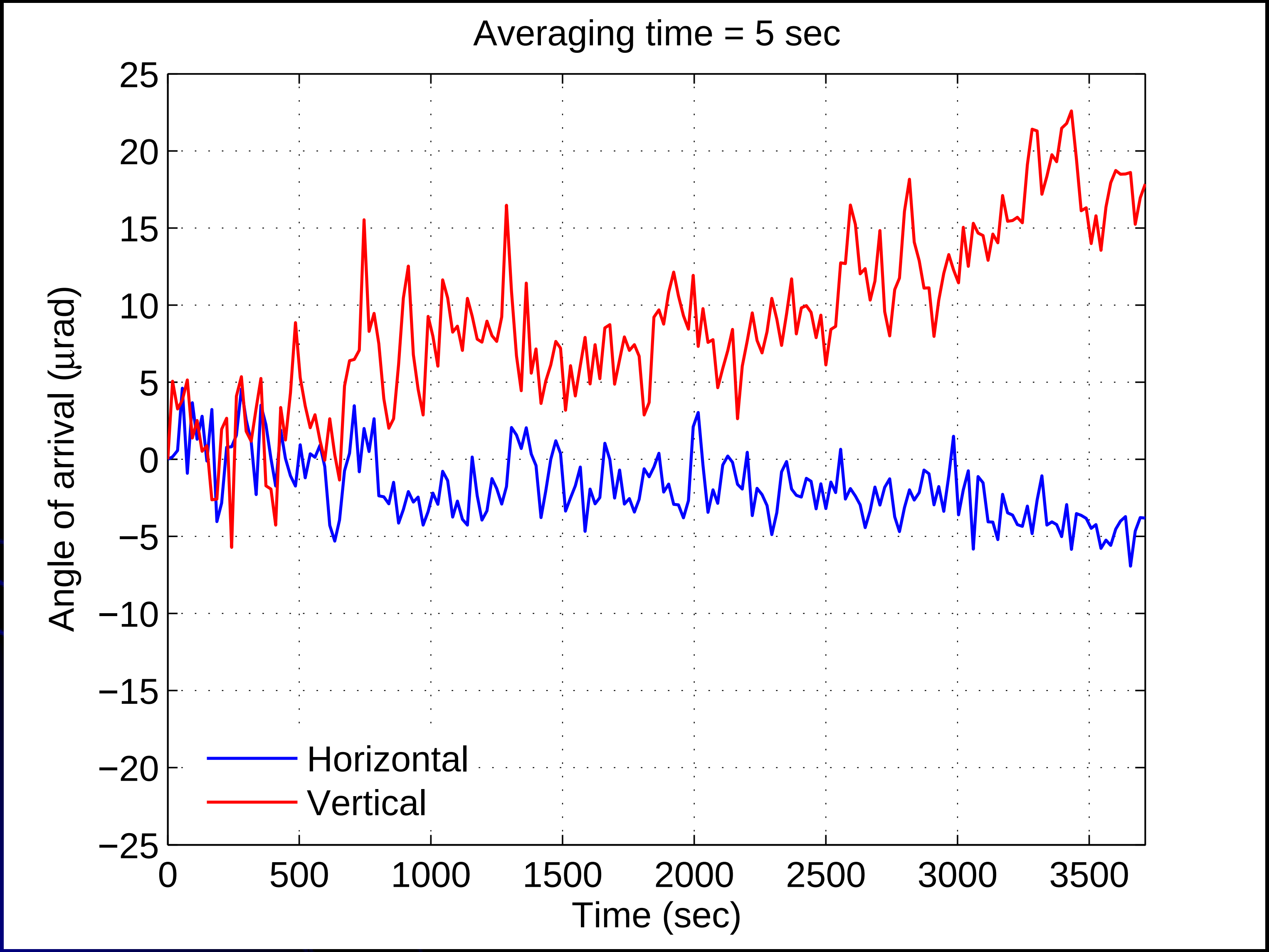

Boulder Atmospheric Observatory, September, 2006

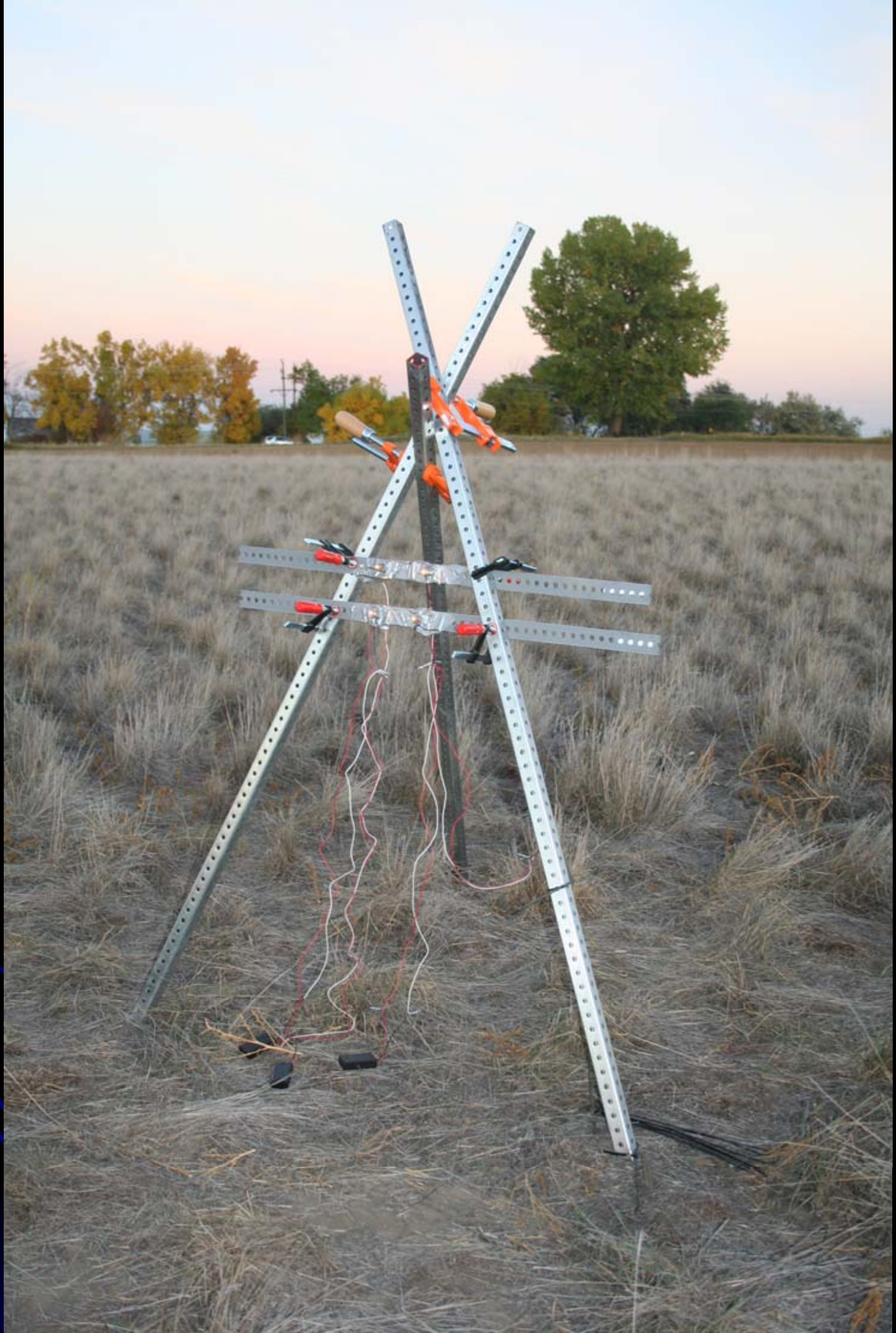

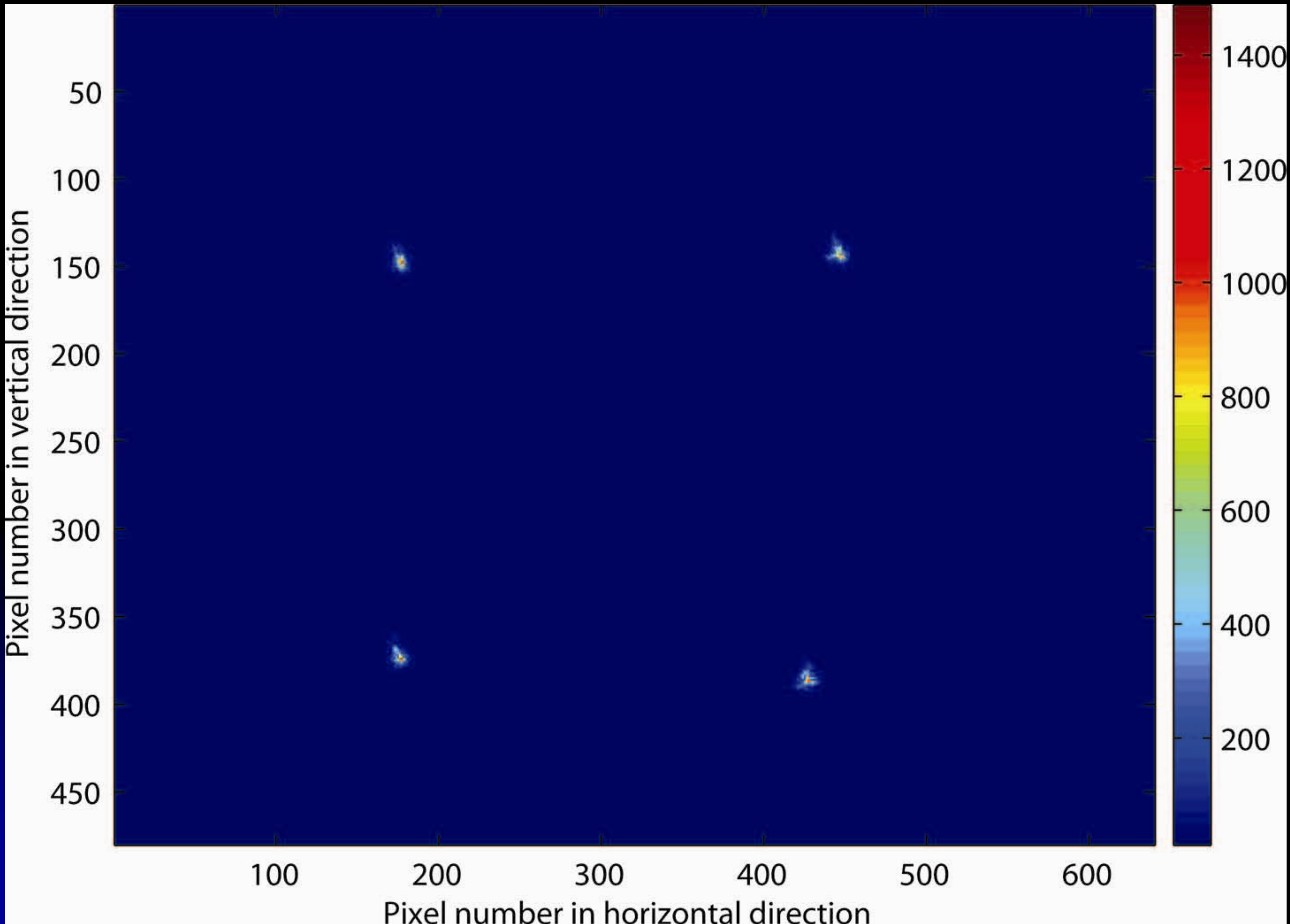
Pixel number in vertical direction
50
100
150
200
250
300
350
400
450
100
200
300
400
500
600
Pixel number in horizontal direction
1400
1200
1000
800
600
400
200

Sequence of snapshots of single light

30 frames / s

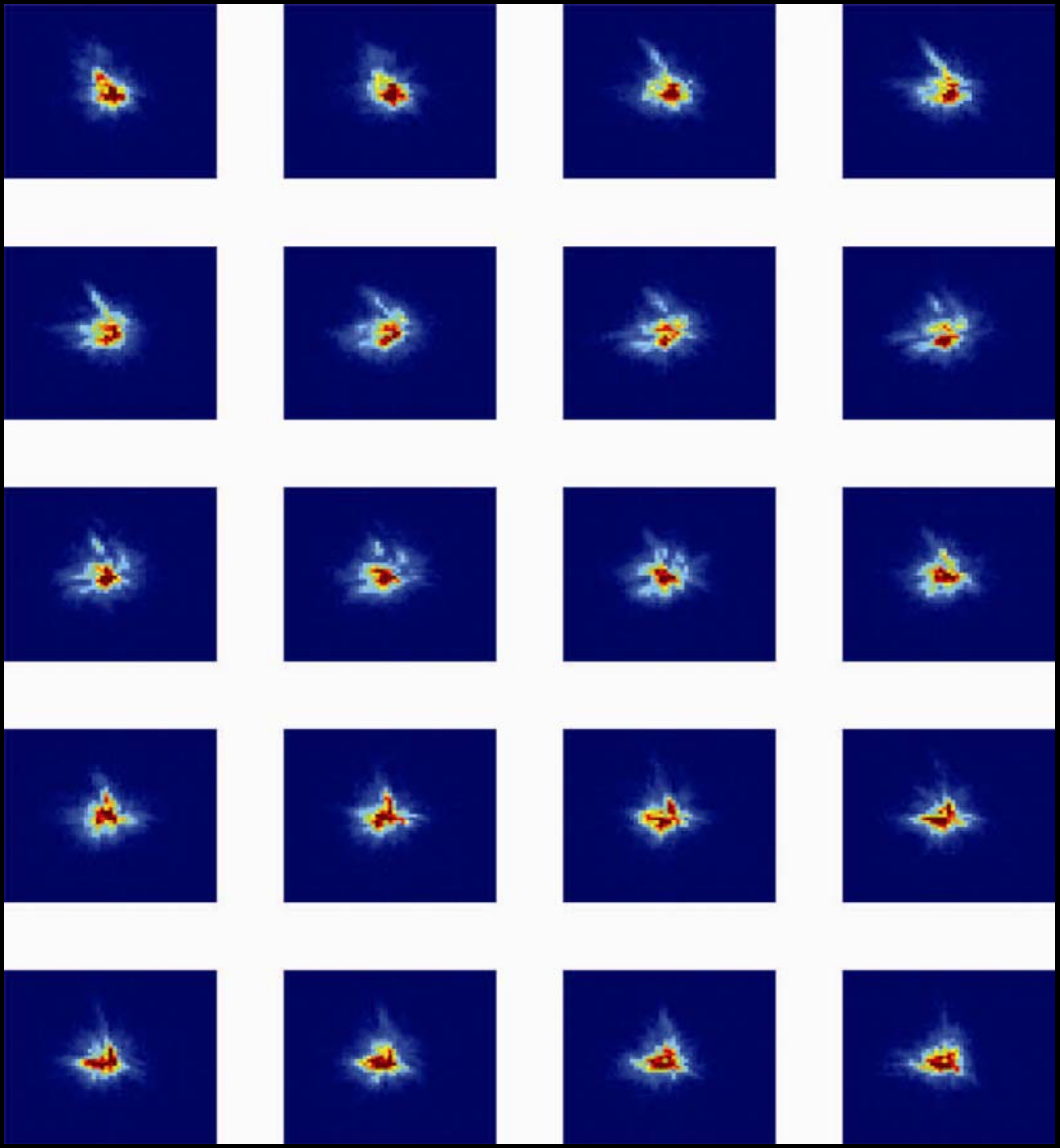

Cheon, Y., V. Hohreiter, M. Behn, and A. Muschinski, 2007: Angle-of-arrival anemometry […]. *J. Opt. Soc. Am. A*, **24**, 3478-3492.

Random ray-bending (lateral and vertical)

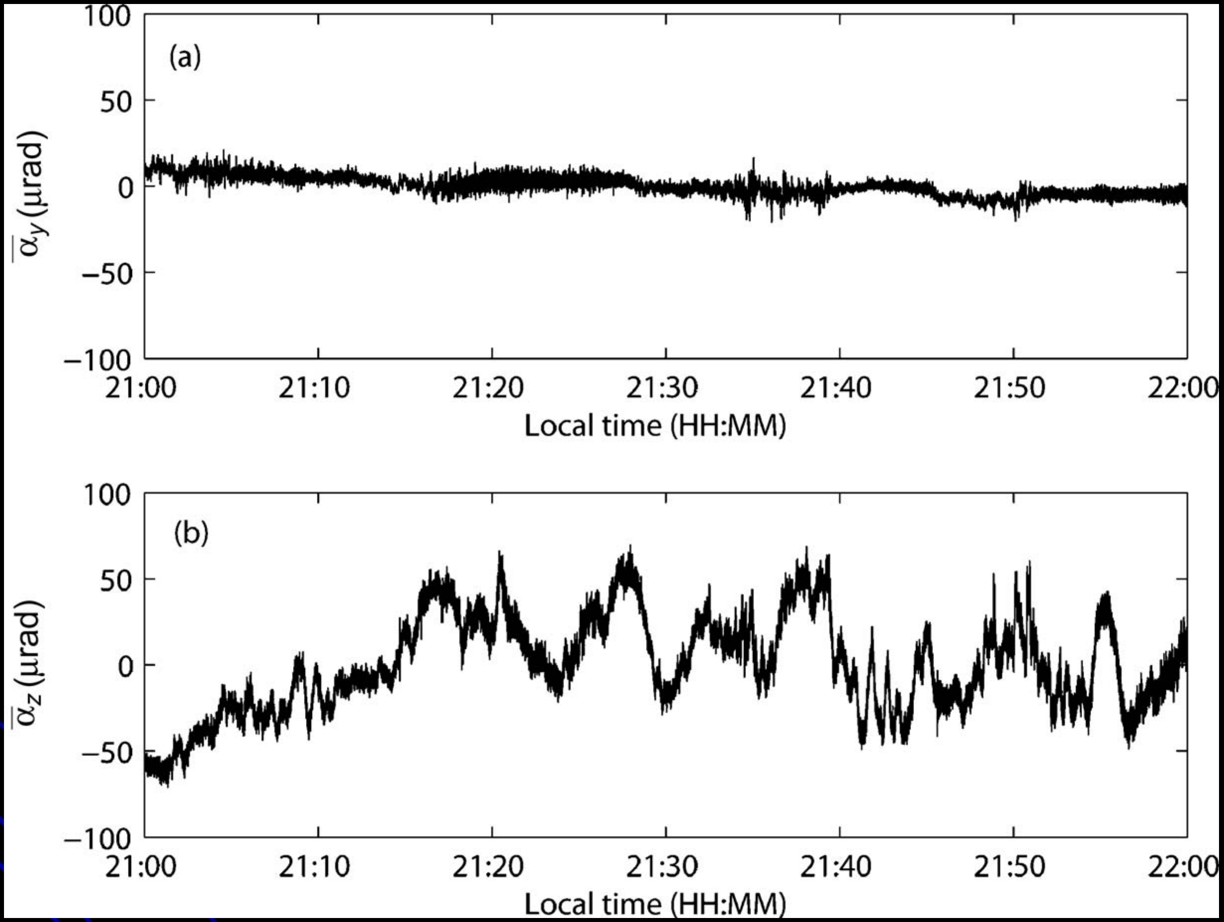

Cheon, Y., V. Hohreiter, M. Behn, and A. Muschinski, 2007: Angle-of-arrival anemometry […]. *J. Opt. Soc. Am. A*, **24**, 3478-3492.

Frequency spectrum of AOA fluctuations

$$S_\alpha(f) = \frac{2^{4/3}}{9\pi^{7/6}\Gamma(5/6)} C_n^2 v_b^{5/3} L b^{-2} f^{-8/3} \left[1 - \frac{\sin(2\pi b f/v_b)}{2\pi b f/v_b} \right], \tag{14}$$

where the numerical coefficient has the value 0.06524. Equation (14) is identical to Clifford's main result, his Eq. (28). [His slightly different coefficient, 0.066, is probably due to rounding errors, and his factor k^2 instead of b^{-2} is due to an erroneous conversion from $W_{\delta S}(f)$ to $S_\alpha(f)$.] It is quite remarkable that Eq. (14) can be easily obtained via the geometrical-optics approximation, Eq. (3), without the cumbersome integrations that Clifford had to carry out because he did not approximate the cosine term as a constant.

Cheon, Y., V. Hohreiter, M. Behn, and A. Muschinski, 2007: Angle-of-arrival anemometry […]. *J. Opt. Soc. Am. A*, **24**, 3478-3492.

Frequency spectrum of AOA fluctuations (measured, lateral and vertical)

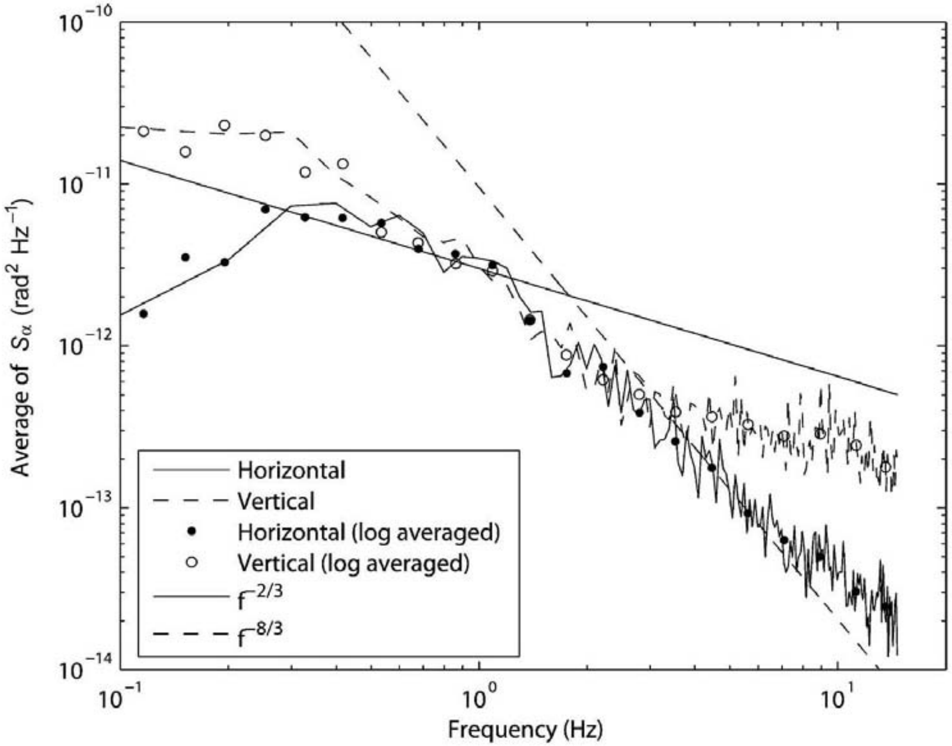

Fig. 7. Averaged frequency spectra of AOA fluctuations for the horizontal direction (solid line) and the vertical direction (dashed line) of the bottom left-hand light measured on September 27, 2006. Each spectrum is for 10 s of time duration. The black dots and open circles are the frequency spectra averaged over intervals of equal logarithmic width for horizontal and vertical directions of 2 min of time duration, respectively. The observation time was 21:20:10–21:22:10 LT.

Cheon, Y., V. Hohreiter, M. Behn, and A. Muschinski, 2007: Angle-of-arrival anemometry […]. *J. Opt. Soc. Am. A*, **24**, 3478-3492.

“Seeing” the wind speed transverse to the line of sight

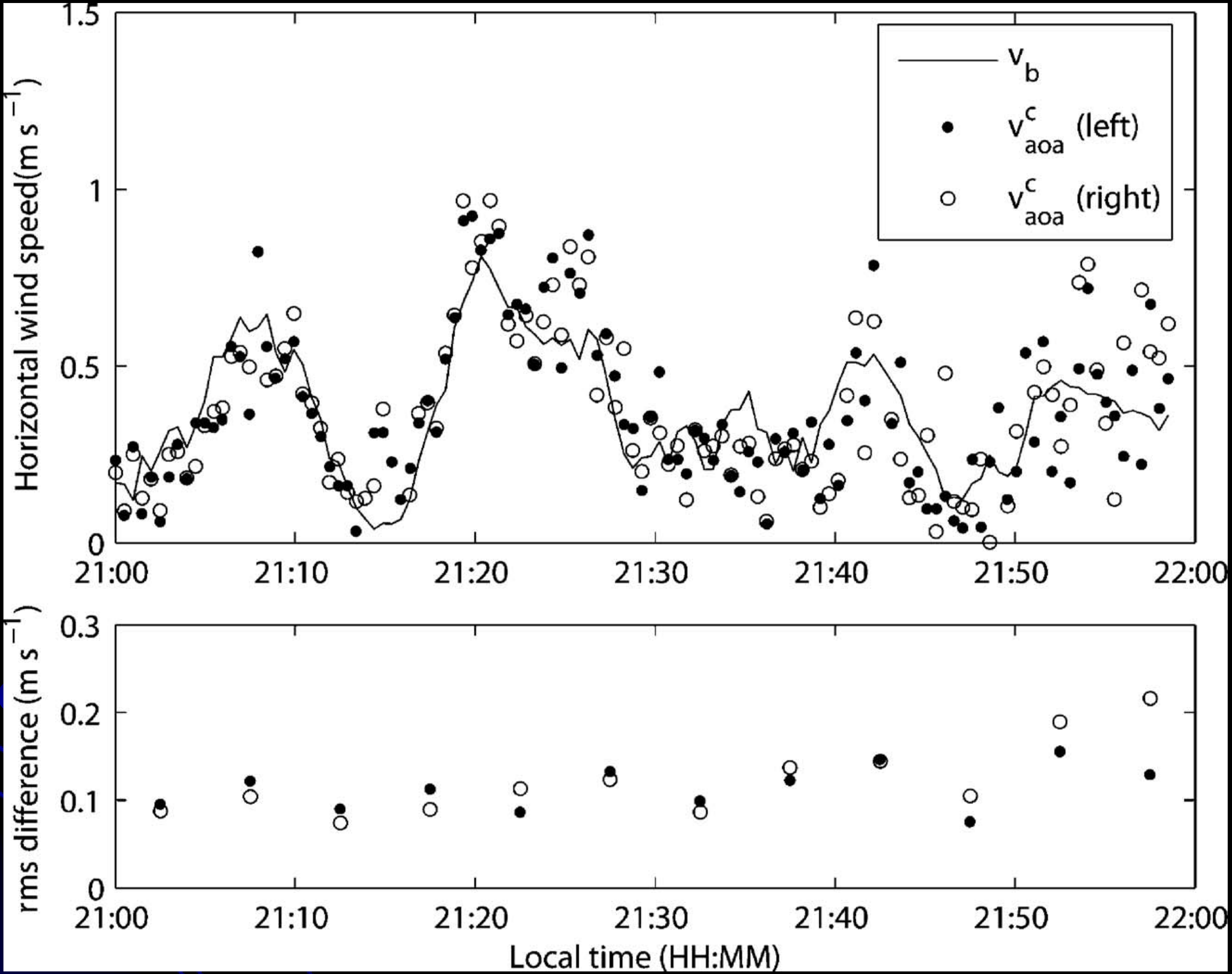

Cheon, Y., V. Hohreiter, M. Behn, and A. Muschinski, 2007: Angle-of-arrival anemometry […]. *J. Opt. Soc. Am. A*, **24**, 3478-3492.

Random ray-bending (lateral and vertical)

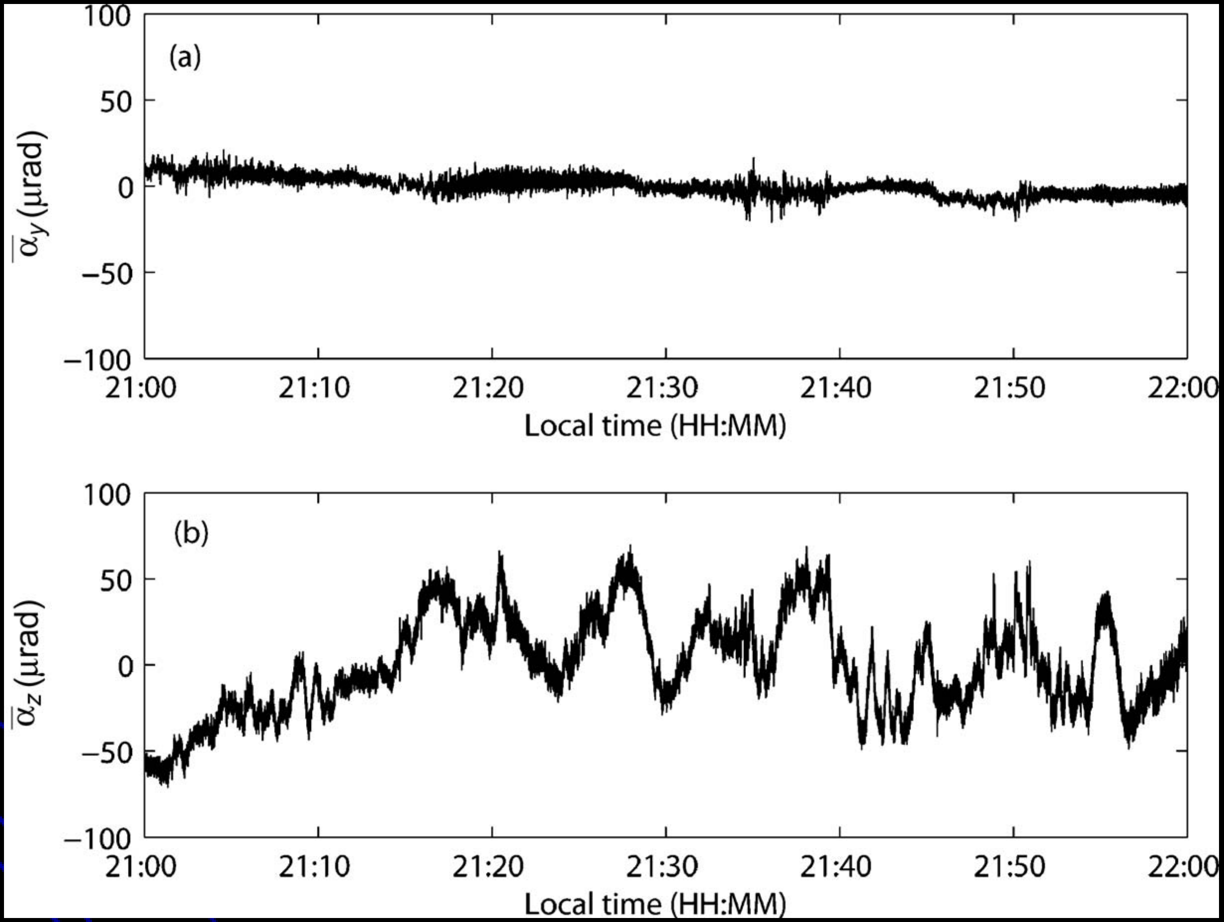

Cheon, Y., V. Hohreiter, M. Behn, and A. Muschinski, 2007: Angle-of-arrival anemometry […]. *J. Opt. Soc. Am. A*, **24**, 3478-3492.

“Seeing” quasi-periodic changes in the vertical temperature gradient (gravity waves)

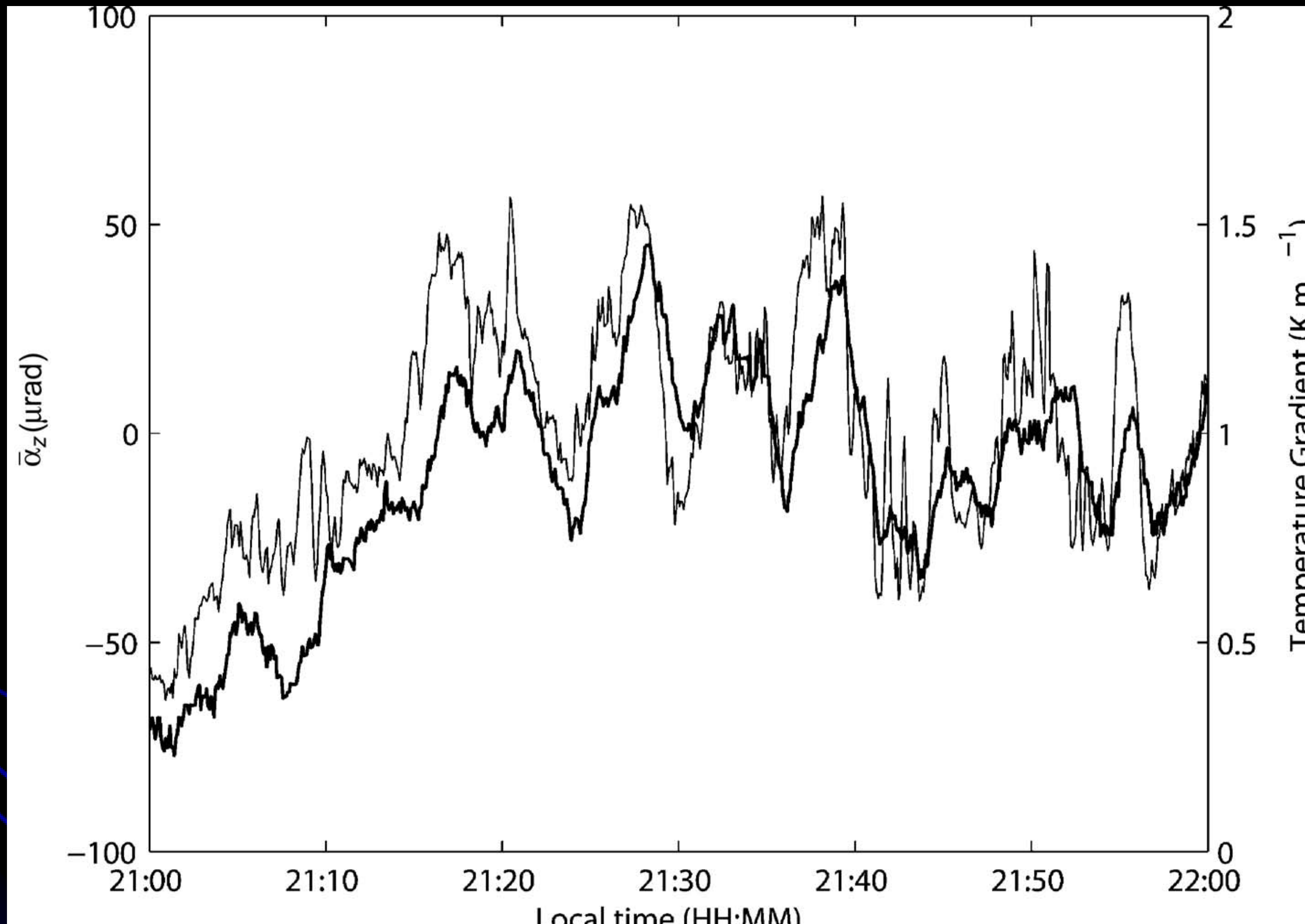

Cheon, Y., V. Hohreiter, M. Behn, and A. Muschinski, 2007:
Angle-of-arrival anemometry […]. *J. Opt. Soc. Am. A*, **24**, 3478-3492.

METCRAX: Looking for "atmospheric seiches" in the Atmospheric Meteor Crater

Overview

- Introduction
- Wave propagation through turbulence: the basics
- Anisotropy in optical surface-layer turbulence
- Vertical-velocity biases observed with radars and sodars
- Outlook

Downward bias in vertical velocities observed with VHF radars in the free troposphere

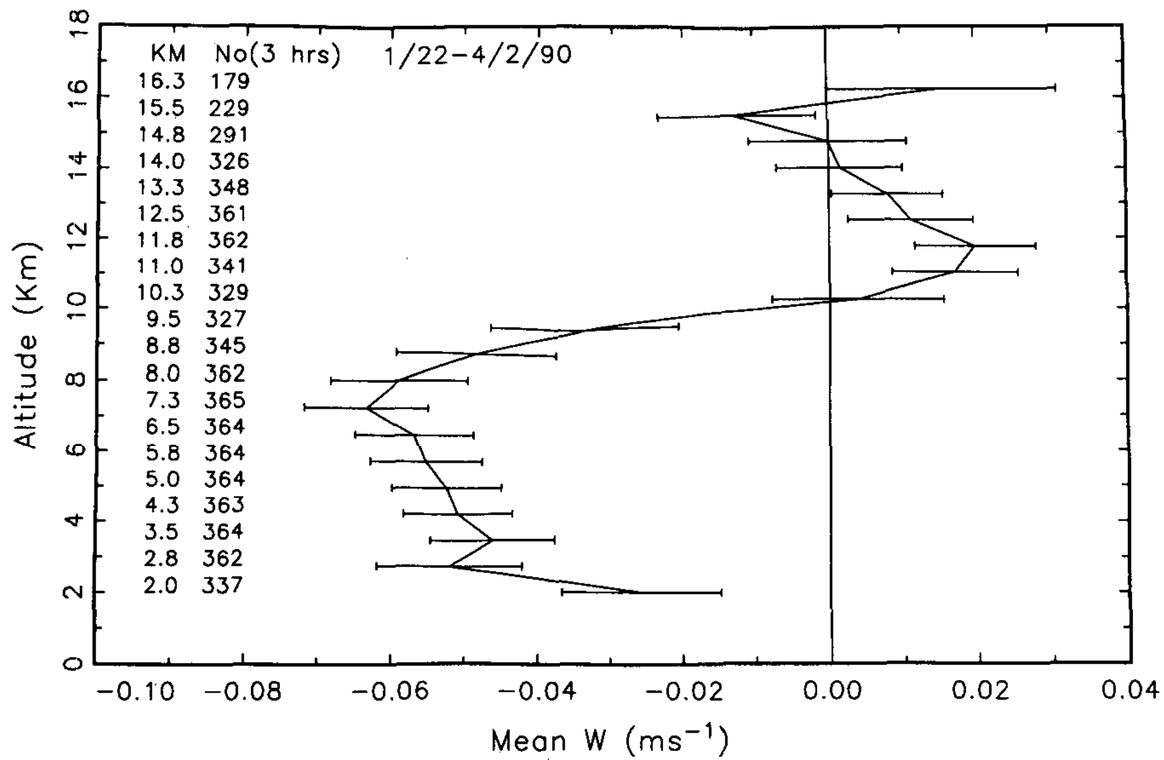

FIG. 2. Vertical profile of the mean vertical velocity at Flatland during 22 January–2 April 1990. The number of 3-h means averaged at each height is given; the error bars extend plus and minus one standard error of the mean.

Nastrom, G. D., and T. E. VanZandt, 1994: Mean vertical motions seen by radar wind profilers. *J. Appl. Meteor.*, **33**, 984-995.

Upward bias in vertical velocities observed with a sodar in the lower CBL

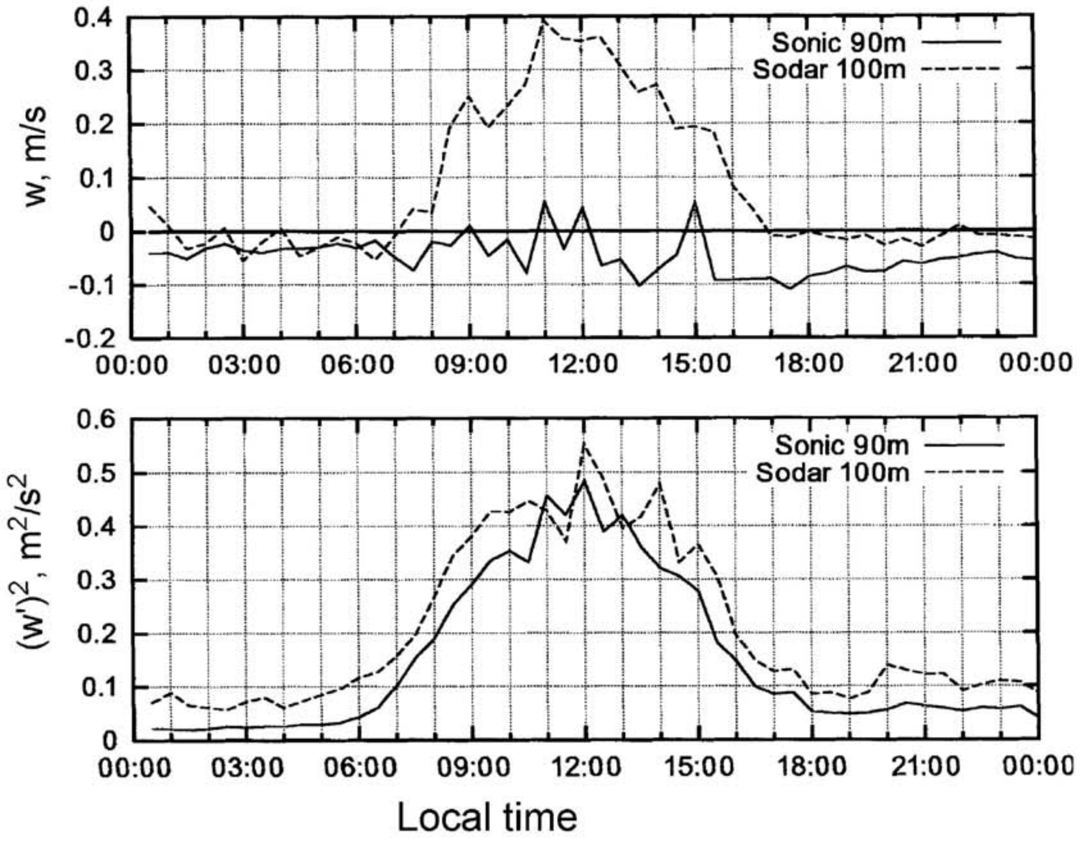

Fig. 2. Comparison of time series of w and σ_w by sonic anemometer and SODAR in convective conditions averaged over nine clear days during September 2000 at Falkenberg, Germany. A moving average of 30 min was used

Coulter, R. L., and M. A. Kallistratova, 2004: Two decades of progress in SODAR techniques […]. *Meteorol. Atmos. Phys.*, **85**, 3-19.

Geophysical causes of biases in vertical clear-air radar or sodar winds

- Nonzero covariance between local Cn2 and local w (due to gravity waves in the stable free troposphere, Nastrom and VanZandt 1994)
- Horizontal advection of asymmetrically corrugated interfaces ("KHI bias", Muschinski 1996)
- Nonzero covariance between local Cn2 and local w ("intermittency flux" or "reflectivity flux" in the CBL, Muschinski et al., to be published)

"KHI bias"

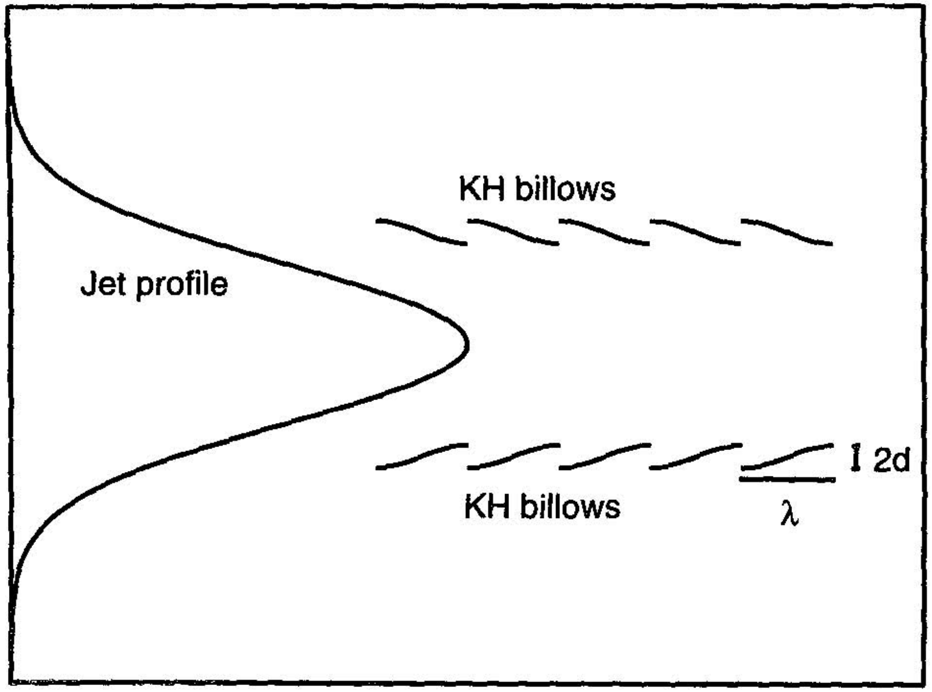

FIG. 1. Geometry of refractivity surfaces in trains of Kelvin–Helmholtz billows above and below the horizontal wind speed maximum of a jet stream (schematic). Note the opposite orientation of the billows above and below the jet.

Muschinski, A., 1996: Possible effect of Kelvin-Helmholtz instability on VHF radar observations of the mean vertical wind. *J. Appl. Meteor*., **35**, 2210-2217.

“KHI bias”

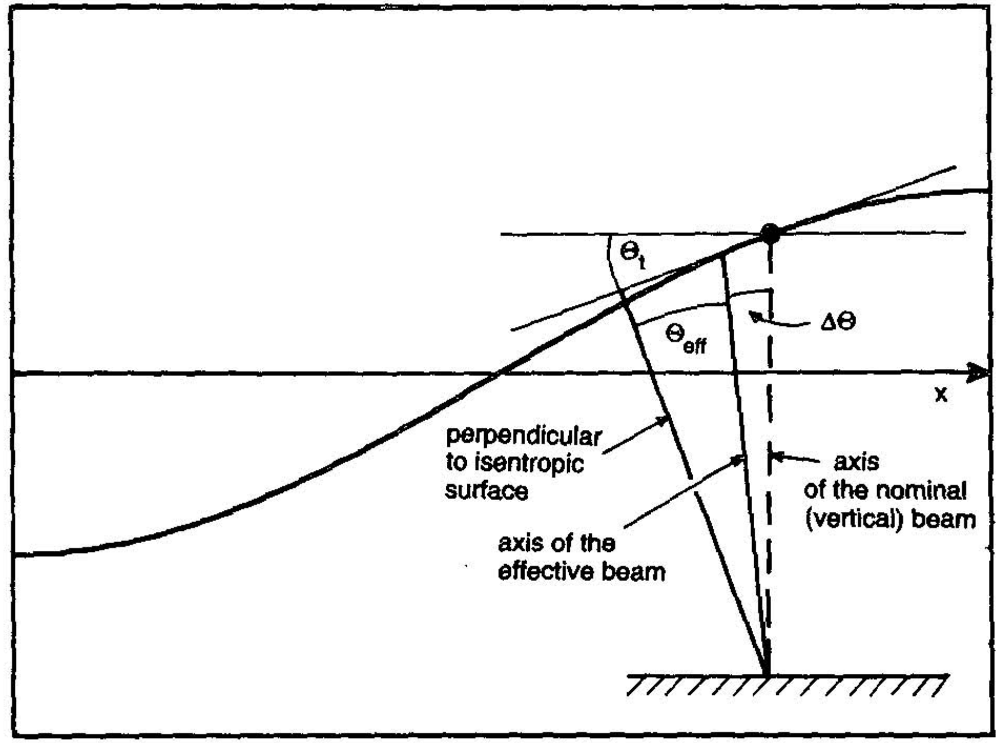

FIG. 2. A sinusoidal quasi-specular refractivity surface in a Kelvin–Helmholtz billow, illuminated by a vertically directed VHF radar beam. Note the difference between the radar's nominal (vertical) and effective beam direction.

Muschinski, A., 1996: Possible effect of Kelvin-Helmholtz instability on VHF radar observations of the mean vertical wind. *J. Appl. Meteor*., **35**, 2210-2217.

Small-scale intermittency:
Lognormality of local epsilon and local CT2

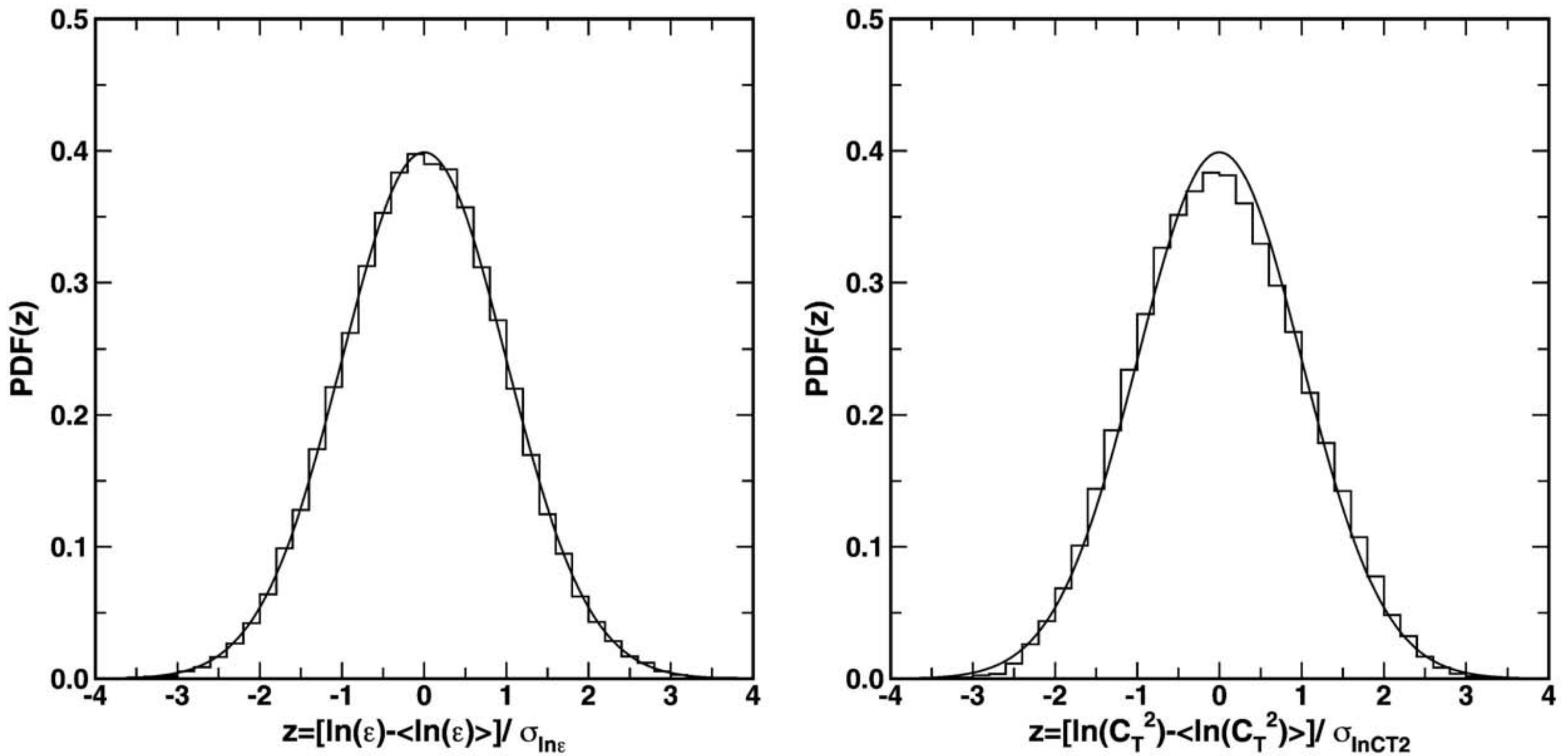

FIG. 3. PDF of $\ln\epsilon$ and the prediction of the lognormal distribution.

FIG. 4. PDF of $\ln C_T^2$ and the prediction of the lognormal distribution.

Frehlich, R. G., Y. Meillier, M. L. Jensen, and B. Balsley, 2004: A statistical description of small-scale turbulence in the low-level nocturnal jet. *J. Atmos. Sci*., **61**, 1079-1085.

Small-scale intermittency: Joint lognormality of local epsilon and local CT2

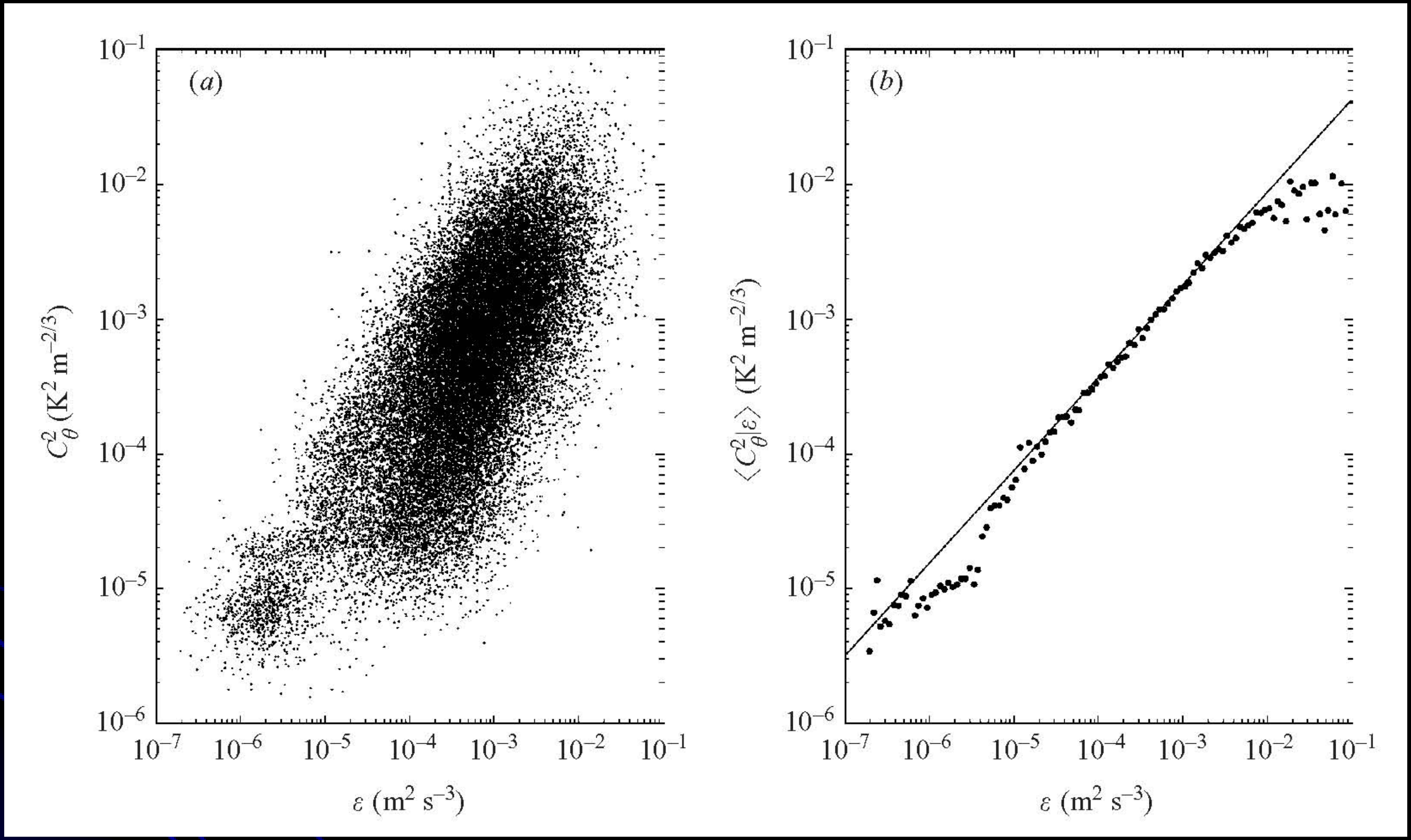

Muschinski, A., Frehlich, and B. Balsley, 2004: Small-scale and large-scale intermittency in the nocturnal boundary layer and the residual layer. *J. Fluid Mech.*, **515**, 319-351.

Intermittency flux and sodar velocity bias

Let $\left(\widetilde{C_T^2}\right)_r$ be the local temperature structure parameter, estimated from a volume of radius r, and let w_r be the vertical wind velocity averaged over the same volume.

Then $\left(\widetilde{C_T^2}\right)_r$ and w_r are random variables, where

$$C_T^2 = \left\langle \left(\widetilde{C_T^2}\right)_r \right\rangle. \tag{1}$$

Then the mean vertical wind velocity measured with a sodar is

$$\langle v_D \rangle = \frac{\left\langle \left(\widetilde{C_T^2}\right)_r w_r \right\rangle}{\left\langle \left(\widetilde{C_T^2}\right)_r \right\rangle} = \langle w \rangle + \frac{\left\langle \left(\widetilde{C_T^2}\right)_r' w_r' \right\rangle}{C_T^2}. \tag{2}$$

Upward flux of local CT2 (sodar reflectivity) in the lower CBL (measured with sonics)

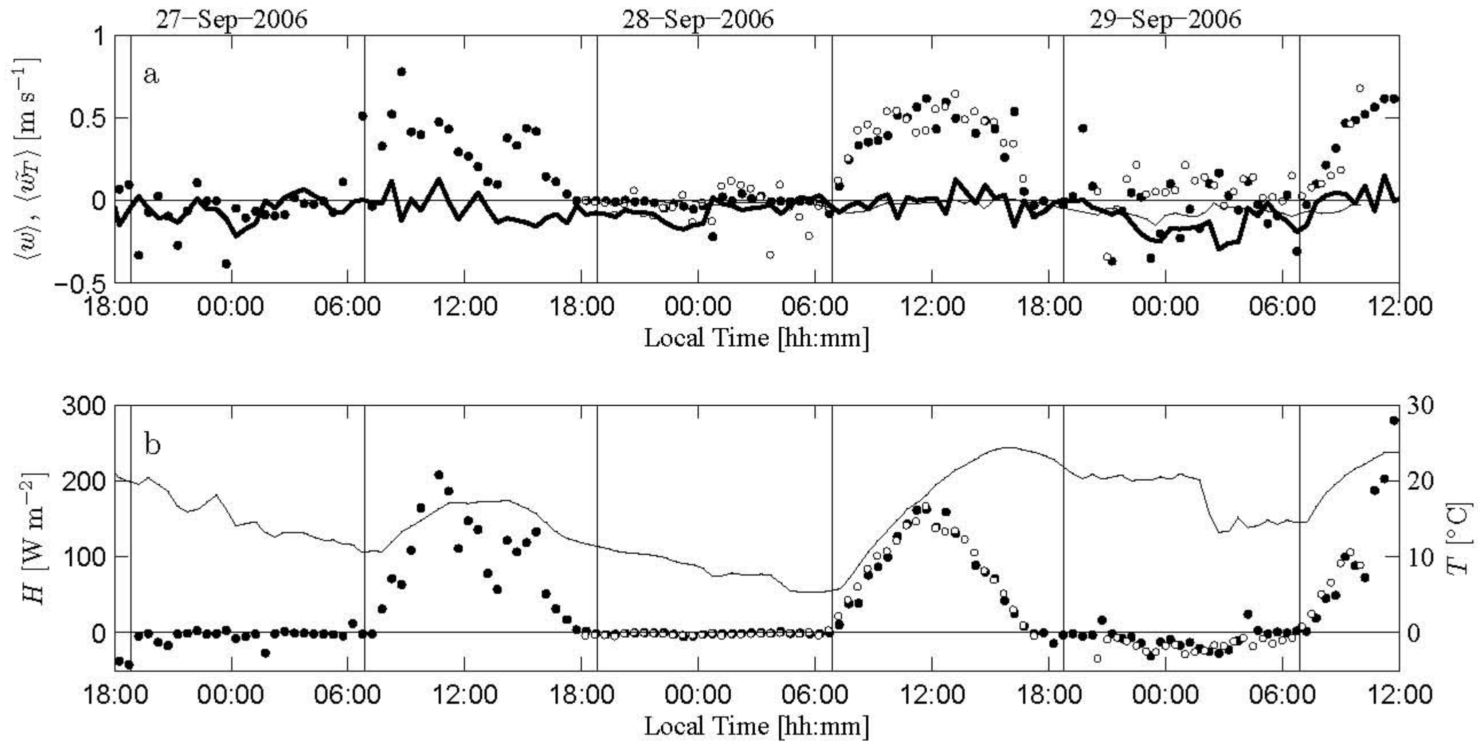

Figure 2. Time series of 30-min estimates of various statistics computed from sonic data collected at the BAO site between 1800 LT on 26 Sep 2006 and 1200 LT 29 Sep 2006. Note that 1.5-m data were collected only after 1800 LT on 27 Sep 2006. (a) $\langle w \rangle$ at 22.5 m AGL (thick solid line) and at 1.5 m AGL (thin solid line), $\langle \widetilde{w_T} \rangle$ at 22.5 m AGL (filled dots) and at 1.5 m AGL (open circles). (b) Sensible heat flux, H, at 22.5 m (filled dots) and at 1.5 m (open circles), air temperature T at 22.5 m AGL (solid line).

Muschinski, A., M. Behn, V. Hohreiter, and Y. Cheon, 2007: Vertical fluxes of the temperature structure variable […]. Unpublished manuscript.

Upward bias in vertical velocities observed with a sodar in the lower CBL

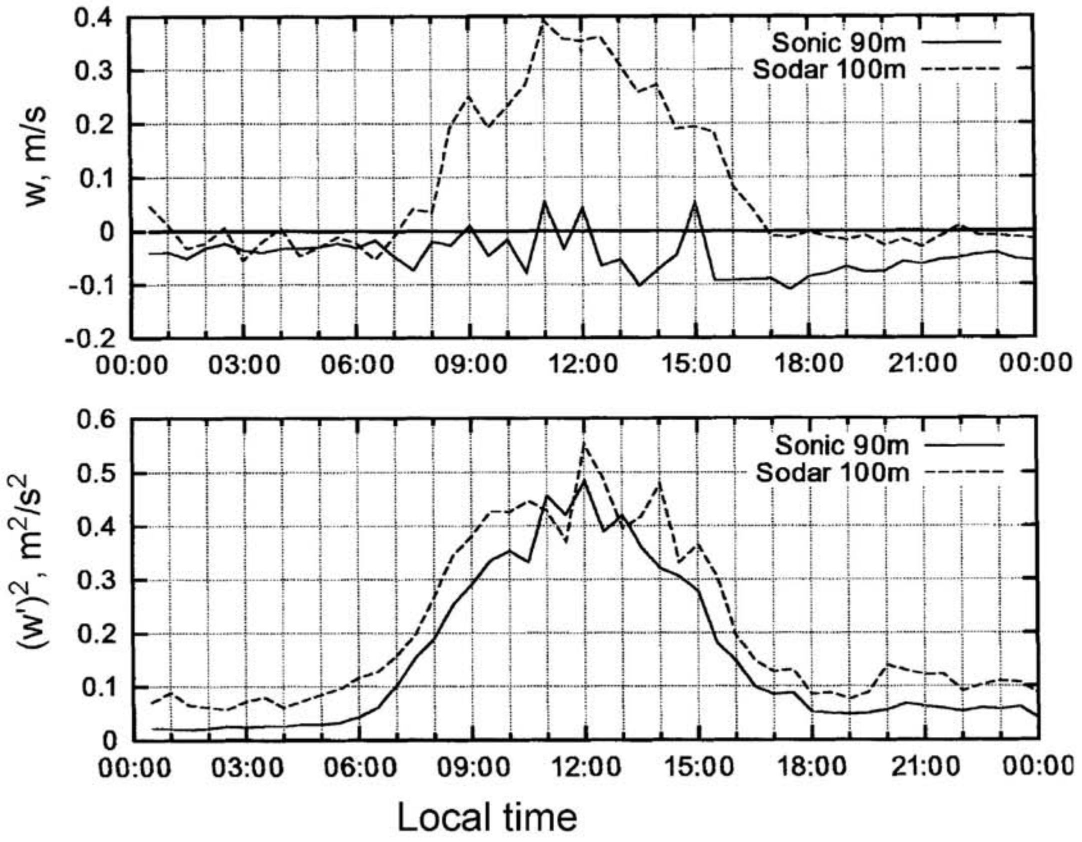

Fig. 2. Comparison of time series of w and σ_w by sonic anemometer and SODAR in convective conditions averaged over nine clear days during September 2000 at Falkenberg, Germany. A moving average of 30 min was used

Coulter, R. L., and M. A. Kallistratova, 2004: Two decades of progress in SODAR techniques […]. *Meteorol. Atmos. Phys.*, **85**, 3-19.

Overview

- Introduction
- Wave propagation through turbulence: the basics
- Anisotropy in optical surface-layer turbulence
- Vertical-velocity biases observed with radars and sodars
- Outlook

Outlook

- Faster data acquisition
- Faster computation
- Better sensors
- Better theoretical understanding
- Better numerical simulations
- Better data assimiliation.

- Better observations and predictions.

Thanks to …

- U.S. Army Research Office (ARO)
- National Science Foundation (NSF)
- NOAA Earth Systems Research Laboratory (ESRL)
- National Center of Atmospheric Research (NCAR)
- Jerry and Linda Paros

… for their generous support!